Arteriovenous malformation animal model for radiosurgery: the rete mirabile.

A A De Salles, T D Solberg, P Mischel, T F Massoud, A Plasencia, S Goetsch, E De Souza and F Viñuela

AJNR Am J Neuroradiol 1996, 17 (8) 1451-1458
http://www.ajnr.org/content/17/8/1451

Arteriovenous Malformation Animal Model for Radiosurgery: The Rete Mirabile

Antonio A. F. De Salles, Timothy D. Solberg, Paul Mischel, Tarik F. Massoud, Andres Plasencia, Steven Goetsch, Evandro De Souza, and Fernando Viñuela

PURPOSE: To study the effects of single-dose radiation on the porcine rete mirabile, a tangle of microvessels that mimics human arteriovenous malformations of the brain. **METHODS:** Eight retia mirabilia received a single dose of radiation under stereotactic location with digital angiography and CT. The following doses were applied: 20, 30, 40, 50, 60, 70, 80, and 90 Gy. The animals were followed up for a period of 7 months. Findings at neurologic examination, serial angiography, and histopathologic examination were analyzed. **RESULTS:** Progressive occlusion as observed by angiography corresponded to the histopathologic finding of intimal hyperplasia; that is, marked thickening of the vessel wall, progressing to occlusion of the vascular lumen, and associated thrombosis. A direct dose response was noted for these changes. Neurologic findings were related to the dose distribution and to histologic findings in structures adjacent to the rete mirabile. **CONCLUSION:** The rete mirabile is an excellent model by which to study the radiologic and histologic effects of single-dose radiation to the microvasculature of the central nervous system.

Index terms: Animal studies; Arteriovenous malformations, cerebral; Radiation, effects

AJNR Am J Neuroradiol 17:1451–1458, September 1996

Arteriovenous malformations (AVMs) of the brain are congenital tangles of abnormal vessels that can cause intracranial bleeding, seizures, severe headaches, progressive neurologic deficits, and a significant decrease in life span by more than 20 years (1–5). Focused single-dose radiation, or radiosurgery, progressively obliterates AVMs within 1 to several years (3, 6–11). The risk of intracranial hemorrhage persists during this period (7, 8, 10), and there is a limit to the size of the AVMs that can be treated successfully. As the size of the AVM increases, the therapeutic dose that can be safely delivered decreases (8, 11, 12). The radiosurgery dose for AVMs has been determined empirically and has not been substantiated experimentally owing to the lack of an experimental model. Better understanding of the effects of radiosurgery on the microvasculature of the central nervous system may lead to strategies for improving the success rate of radiosurgery and to a decrease in the complication rate (13, 14). This article describes an experimental animal model that serves to study radiosurgical dose and radiation sensitizers, as well as radiologic, histologic, and radiobiological changes brought about by radiosurgery to a conglomerate of microvessels resembling a human AVM of the brain.

Received December 11, 1995; accepted February 19, 1996.

Supported in part by an Academic Senate grant from the University of California, Los Angeles.

From the Division of Neurosurgery (A.A.F.D.S.) and the Departments of Radiation Oncology (T.D.S., S.G.), Pathology and Laboratory Medicine (Neuropathology) (P.M.), and Radiological Sciences (T.F.M., A.P., E.D.S., F.V.), University of California at Los Angeles, School of Medicine.

Address reprint requests to Antonio A. F. De Salles, MD, PhD, Division of Neurosurgery, 300 UCLA Medical Plaza, Suite B-212, Los Angeles, CA 90024.

AJNR 17:1451–1458, Sep 1996 0195-6108/96/1708–1451

Materials and Methods

Animal Preparation

Four Red Duroc swine weighing 20 to 40 kg were anesthetized. Diazepam (0.5 to 1 mg/kg) was injected intramuscularly, and endotracheal intubation was performed. Halothane (1% to 1.5%) was used to maintain the anesthesia. A stereotactic frame designed for the swine and compatible with the Brown-Roberts-Wells (BRW) system (Radionics Co, Burlington, Mass) was attached to the animals' head (15). A local anesthetic was injected bilater-

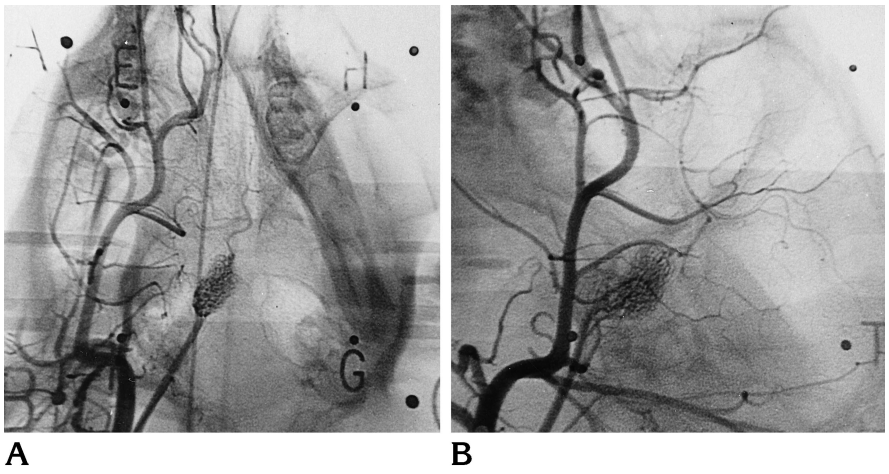

Fig 1. Anteroposterior (*A*) and lateral (*B*) views of a stereotactic angiogram of the rete mirabile. The ascending pharyngeal artery feeds the rete mirabile. The largest artery is the external carotid artery, the small artery draining the rete mirabile is the internal carotid artery (center of the figures). For detailed anatomy see Manchola et al (4). The dimensions and target coordinates of the retia were identified on the angiogram and transferred to the CT scans.

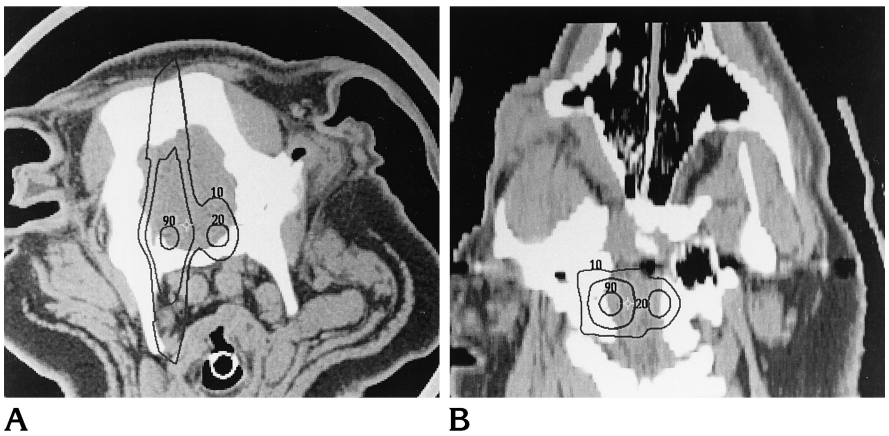

Fig 2. Radiosurgical plan displayed on coronal (*A*) and axial (*B*) reconstructed CT scans. Notice the 90% isodose line covering the left rete and the 20% isodose line covering the right rete (animal 1, Table 2). The coronal view shows that there was large spread of the 20% isodose line around the left rete as well as high levels of radiation to structures located between the retia (*star*). Isodose lines were normalized to 100%. There was, however, a high degree of homogeneity throughout each rete (see Table 2).

ally in an area over the angle of the jaw and in two areas over the scalp. The screw pins that held the stereotactic frame in place were attached to these sites. The BRW stereotaxic ring was attached to the swine frame. Angiographic and computed tomographic (CT) localizers were used during imaging acquisition.

Imaging Acquisition

The angiographic technique for imaging the swine has been described in a previous article (16). Briefly, the animal's groin was sterilized, the femoral artery was punctured and catheterized by a standard Seldinger technique, and a 5.5F to 4F Viñuela catheter (Cook, Bloomington, Ind) was guided cephalad under fluoroscopy. The right and left common carotid arteries were then selectively catheterized, and angiographic films showing the right and left retia in anteroposterior and lateral views were obtained (Fig 1). The animal was transferred to the CT suite, where 3-mm-thick coronal sections were obtained. The orientation of the animal's brain in relation to the CT gantry was coronal because of the orientation of the stereotactic frame (Fig 2). The data obtained were transferred by magnetic tape to the radiosurgery planning computer. The CT scan was used to define the contour of the animal's head, necessary for calculating beam attenuation (17).

Radiosurgery Procedure

The radiosurgery planning was developed by using the SRS-200 Philips software (Philips Medical Systems, Shelton, Conn) (8). Fiducials of the angiographic localizing box and the outline of each rete mirabile were digitized into the planning computer. The dimensions and the stereotactic coordinates of the rete mirabile were obtained by using anteroposterior and lateral angiographic views (Table 1). These dimensions could not be appreciated on CT scans because of the proximity of the rete mirabile to the bone of the skull base. The isocenter coordinates were transferred to the CT scan and the dose distribution was displayed in a multiplanar fashion. Dimensions obtained from a pair of anteroposterior and lateral films tend to overestimate the axial size of the rete mirabile (18, 19).

The radiosurgery treatment plan was developed to cover both retia mirabilia in each animal. A single isocenter, with a 12-mm-diameter collimator, was used on each rete mirabile. Output of collimators as small as 10 mm in diameter have been shown to be accurate to better than 5% (20). The peripheral dose delivered to each rete mirabile varied from 20 to 90 Gy in 10-Gy increments (Table 2). The desired dose distribution to each rete was obtained by selective weighting of arcs (21). Because there was overlapping of dose distribution between right

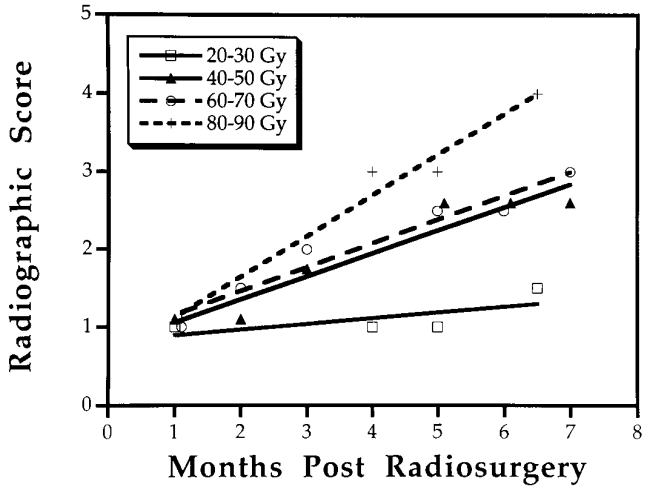

Fig 3. Linear regression of the angiographic response over time related to radiosurgical dose. The curves *20–30 Gy* and *80–90 Gy* are significantly different ($P < .05$).

TABLE 1: Dimensions of the rete mirabile in four swine

Animal	Dimension, cm			Volume, cm^2*
	Lateral	Anteroposterior	Axial	
1 L	1.2	1.7	2.0	2.13
R	1.5	1.7	1.9	2.54
2 L	1.5	1.8	2.0	2.83
R	1.3	1.6	2.0	2.18
3 L	1.3	2.0	2.0	2.72
R	1.4	1.9	2.0	2.79
4 L	1.4	1.8	2.1	2.77
R	1.4	2.1	2.0	3.08
Mean	1.38	1.83	2.00	2.63
SD	0.01	0.16	0.05	0.31

* Volume was calculated by using the formula $V = 4/3\Pi \times L/2 \times AP/2 \times A/2$.

and left retia mirabilia, the dose to the brain stem, hypothalamus, pituitary, hippocampus, and cranial nerves was significant in some animals (Fig 2). This was allowed to permit the study of neurologic and histologic changes in structures related to the rete mirabile. A high degree of homogeneity in dose distribution throughout each rete was, however, the goal of the radiosurgery planning (Table 2).

Neurologic and Radiologic Follow-up

Animals were observed weekly for 10 minutes during their regular activities. The activity level in the cage was noted by simple observation. Quantification of this activity was not performed. The animal's use of extremities, balance, drive for food, corneal reflex, eye movements, and pupillary response to light were checked. Abnormal activities such as seizures, rotatory behavior, and persistent scratching on the cage walls were registered. Animals were examined at least every 2 months with digital subtraction angiography. The volume and density of the rete mirabile were analyzed. Stenosis of feeding and draining vessels was measured. The radiation effects on the radiologic aspect of the rete mirabile were graded from zero to four, zero representing no effect and four maximal effect.

TABLE 2: Parameters for radiosurgery in four swine

Animal	Prescription Percentage of Isodense Line	Peripheral Dose, Gy	Maximum Dose, Gy	Homogeneity, %*
1 L	90	90	100	11
R	20	20	22	10
2 L	90	80	89	11
R	33	30	35	16
3 L	90	70	78	11
R	51	40	45	13
4 L	90	60	67	12
R	75	50	54	8

* Five arcs were used for each rete. Arcs were weighted to obtain the desired dose distribution; a 12-mm collimator was used for each rete mirabile. Homogeneity was calculated by using the formula Homogeneity % = [(Maximum dose − Peripheral dose)/Peripheral dose] × 100.

Histopathologic Studies

Animals were killed by barbiturate overdose. The skull was removed and the retia mirabilia recovered intact for histologic analysis. The relationship of the rete mirabile to the cranial nerves and base of the brain, as well as its macroscopic aspect, were documented by photographs. The retia mirabilia, cranial nerves, and brain were fixed in 10% buffered formaline for a minimum of 2 weeks. After gross examination, the brain was sectioned coronally, and sections of brain, retia mirabilia, and cranial nerves were obtained for light microscopic examination. Paraffin-embedded material was stained with hematoxylin-eosin and examined by the neuropathologist, who was unaware of the dose of radiation received by each rete mirabile. The histologic findings were graded from zero to four, zero being no change and four maximal change.

Statistical Analysis

Paired and unpaired *t* tests were used to compare parametric data. Significance was considered at the $P < .05$ level.

Results

Neurologic Findings

All animals had some neurologic dysfunction, as all received a minimum of 60 Gy to the left rete mirabile (Table 3). Findings in those receiving lower doses included slight right-sided

TABLE 3: Severity of symptoms in response to radiation dose in four swine

Animal	Hemiparesis	Ocular Motor Function	Visual Function	Seizure
1	Severe	Moderate	Moderate	Severe
2	Severe	Severe	Severe	...
3	Moderate	Mild	...	...
4	Mild	...	...	...

TABLE 4: Dose delivered to structures related to the rete mirabile

		Animal			
		1	2	3	4
		Gy (%)	Gy (%)	Gy (%)	Gy (%)
Cerebral peduncle	L	80 (80)*	71 (80)*	62 (80)*	53 (80)*
	R	15 (15)†	22 (25)	35 (45)	47 (70)*
Pituitary		20 (20)	18 (20)	16 (20)	13 (20)
Hippocampus	L	40 (40)*	36 (40)	31 (40)†	26 (40)
	R	15 (15)	22 (25)	35 (45)	37 (55)
Cavernous sinus nerves	L	95 (95)*	84 (95)*	74 (95)*	63 (95)
	R	25 (25)	36 (40)	43 (55)†	53 (80)
Trigeminal ganglion	L	85 (85)*	75 (85)*	65 (85)*	56 (85)
	R	15 (15)	22 (25)	35 (45)	37 (55)†

Note.—% indicates prescription isodose line; dose described is within 5% of the isodose line to the structures.

* Detected symptoms related to the structures.

† Lowest dose leading to abnormal histologic findings.

hemiparesis and some loss of coordination and impaired eye movements on the left side. These complications were relatively minor and the animals were followed up for a period of 7 months and were killed on schedule. Animals receiving greater than 70 Gy to the left side had more severe symptoms related to the structures in the vicinity of the rete mirabile (Table 4). Eye movement dysfunction was the most common finding, since the cranial nerves III, IV, and VI are in close relationship to the rete mirabile. One animal had blindness in one eye. The radiosurgical dose for this animal's ipsilateral rete mirabile was 80 Gy. The animal that received the highest dose, 90 Gy, had severe right-sided hemiparesis and seizure episodes. The animals with severe hemiparesis, blindness, or seizures were killed prematurely.

Angiographic Findings

During the first 2 months after radiosurgery, few angiographic changes were observed, despite the different doses delivered. Retia mirabilia that received more than 50 Gy showed a substantial (50% or greater) decrease in vascularity 4 to 5 months after radiation. The vascular density at 5 months was inversely proportional to the radiation dose delivered (Fig 3). The rete mirabile in the animal that received 90 Gy was almost completely obliterated at 5 months. Narrowing of the vessel feeding the rete was observed in parallel with its disappearance. The existing vessel displayed the same phenomenon observed in the feeding vessel (Fig 4).

Histopathology

The radiated rete mirabile exhibited a spectrum of pathologic changes. Intimal hyperplasia, consisting of marked proliferation of the intima with progressive occlusion of the lumen, was prominent in small arteries and arterioles (Fig 5). These observations exhibited a direct correlation with the dose of radiation. Vascular thrombosis paralleled hyperplasia (Fig 6). Other associated changes included perivascular inflammation in a predominantly perivenous distribution, dystrophic microcalcification, and hemosiderosis. None of these changes showed a clear relationship to the radiosurgical dose.

The peduncle was affected in every animal studied; overt necrosis was observed with doses above 50 Gy. The peduncular region that received 80 Gy showed a large region of hemorrhagic necrosis surrounded by a region of gliosis, foamy microphages, edema and axonal swelling, thickened and hyalinazed blood vessels with a rim of inflammatory process, and astrocyte atypia. The intensity of this finding was similar at doses above 50 Gy. Histologic changes in intracavernous sinus cranial nerves started to appear with doses above 53 Gy. These changes consisted of inflammatory processes with edema, microphages, lymphocytes, macrophages, and eosynophils. Doses above 70 Gy led to demyelinization, inflammatory processes, and lymphocytic vasculitis. The gasserian ganglion showed histologic changes at doses above 35 Gy. At a dose of 35 Gy, mild lymphocytic infiltration was seen; however, at a dose of 65 Gy, a severe inflammatory process with vascular wall thickening and thrombosis was observed. The maximal dose delivered to the pituitary gland was 20 Gy. There were no histologic changes in the pituitary gland at these doses. The hippocampus showed mild inflammatory processes at a dose of 36 Gy and a small infarct involving the dentate giros and

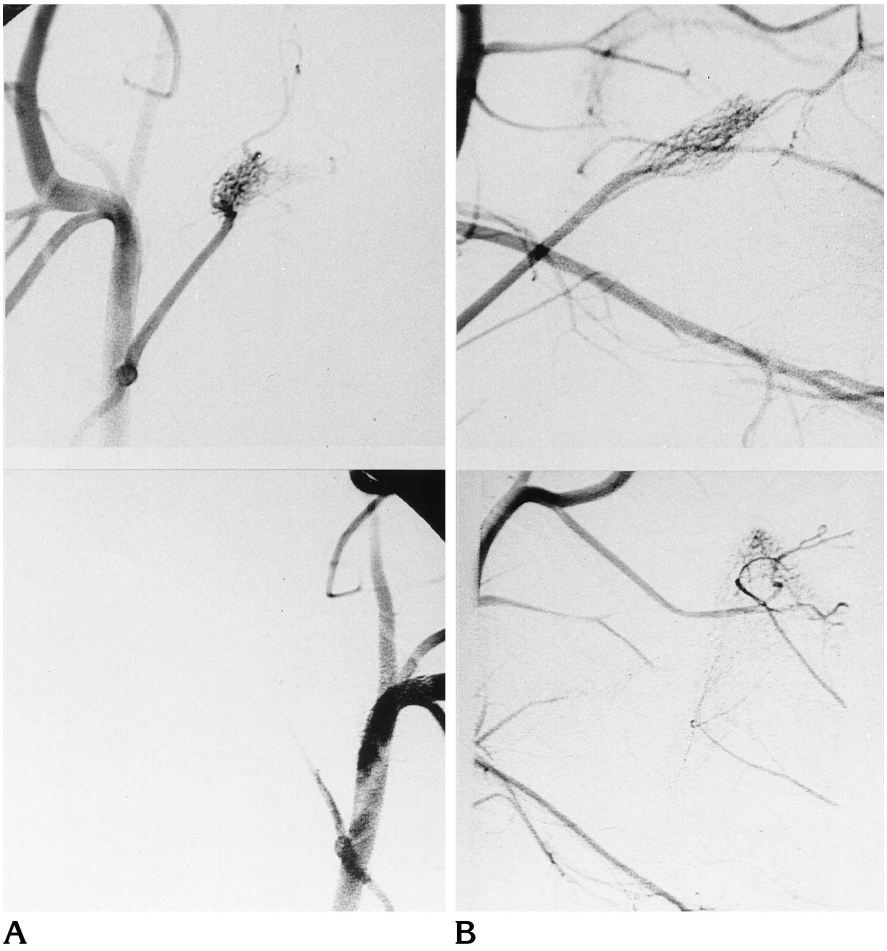

Fig 4. Digital angiography 6 months after radiosurgery, anteroposterior (*A*) and lateral (*B*) views (compare with Fig 2). Upper images represent the rete mirabile that received 20 Gy, lower images show the almost complete disappearance of the rete that received 90 Gy. Notice the narrowing of the ascending pharyngeal artery exiting the common carotid artery seen in the lower right corner of *A* (upper image).

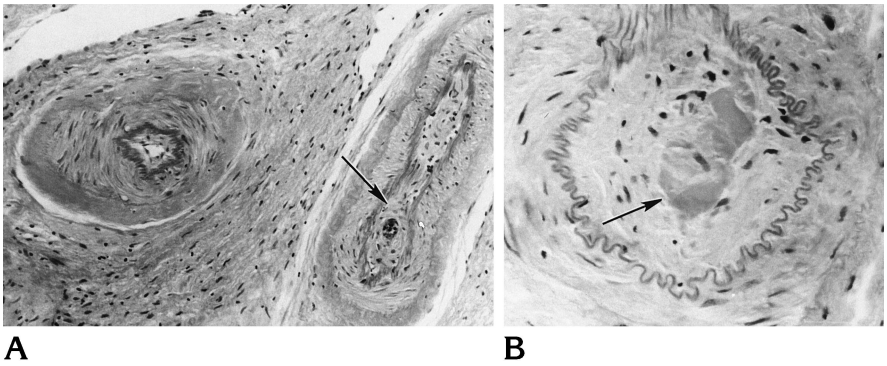

Fig 5. Photomicrographs show thickening of vessel wall (*A*) consisting of hyperplasia of intimal muscular cells and fibroblasts (*arrow*), transverse and longitudinal views, and complete thrombosis of the vascular lumen (*B*) (*arrow*).

CA3 region at a dose of 40 Gy, which was the highest dose delivered to the hippocampus.

Discussion

This work validates the usefulness of an animal model for the study of single-dose radiation effects to a central nervous system vascular structure that mimics AVMs of the brain treated by radiosurgery (3). The swine's rete mirabile possesses several attributes of an AVM candidate for radiosurgery. It is a tangle of microarteries and arterioles fed and drained by large blood vessels. The diameter of the rete microvessels, an average of 154 μm (22), is close to the diameter of vessels composing an AVM nidus, an average of 265 μm (23). The rete is in close relationship to vital structures of the animal's brain. The effects of radiation to the vasculature can be followed up by means of angiography, as demonstrated. The effects of

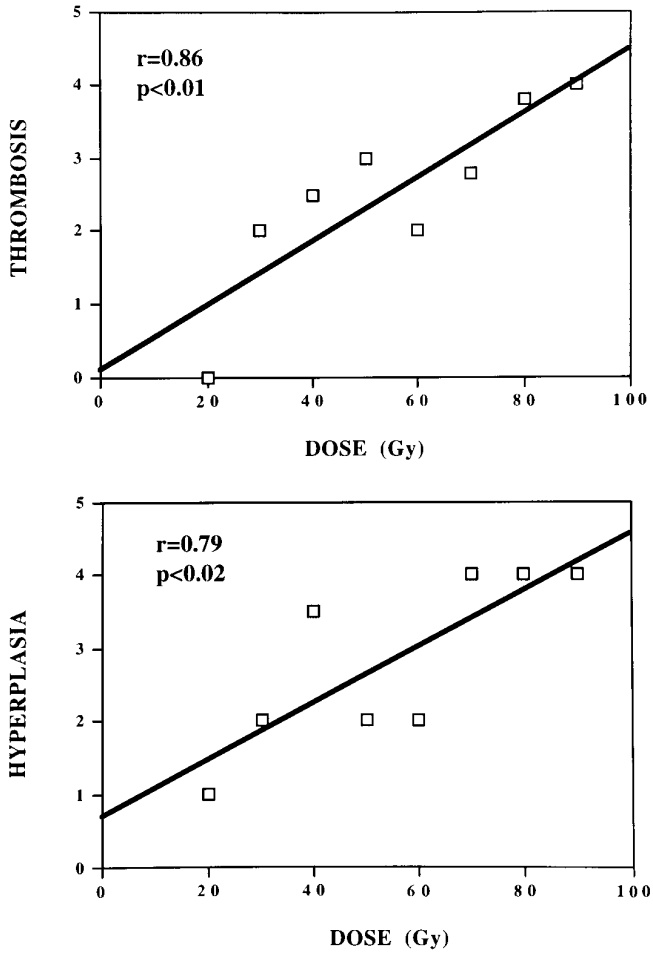

Fig 6. Thrombosis paralleled hyperplasia and was directly proportional to the dose delivered.

radiation to adjacent structures can be followed up by means of neurologic examination and confirmed with histologic studies. Effects to adjacent structures can also be followed up over time by CT.

An important distinction between the hemodynamics of the rete mirabile and those of human AVMs is the difference in the blood pressure across these two structures. The rete is an arterioarterial system, while the AVM is an arteriovenous system and thus has a higher pressure gradient between feeding and draining vessels than the gradient observed in the rete (24, 25). The importance of this pressure gradient on the obliteration rate of AVMs or of the rete mirabile after radiosurgery is unknown. This question is under investigation in our laboratories (26). The histologic difference between the rete, including the lack of venules in the body of the rete mirabile, and human AVMs is another important factor against using the rete mirabile as a model for AVMs.

Neurologic Findings

Few experimental studies have evaluated clinical changes after radiosurgery. We observed hemiparesis, blindness, eye movement deficits, seizures, and slow development in the animals we studied. The rete mirabile is situated within the cavernous sinus (19) and therefore in proximity to structures related to these neurologic manifestations. There was no intention to avoid these structures when the radiosurgery plan was developed. The only criterion for plan selection was complete coverage of both retia. This was accomplished with a high degree of homogeneity within each rete. The coverage of both retia with a substantial and homogeneous radiation dose led to superimposition of the isodose lines outside the retia with consequent high-dose radiation delivered to structures near the retia. The importance of homogeneity when covering an AVM has been a matter of controversy. Groups using linear accelerator or particle beam-based radiosurgery tend to prescribe a more homogeneous dose distribution to the nidus, with approximately a 20% difference between the peripheral and the central dose (8, 12). On the other hand, groups using the gamma unit tend to prescribe a less homogeneous dose to the nidus, with approximately a 50% difference between the peripheral and the central dose (9). This animal model offers the opportunity to study this issue in future experiments.

The function of the rete mirabile is poorly understood. The following hypotheses have been formulated to explain its presence in some animals: thermal exchange in the brains of the camel and whale, hemodynamic regulation in the whale and giraffe, collateral anastomosis in all of them, monitoring of air humidity in goats, and a source of extrapulmonary gas exchange for improvement of brain oxygenation in birds (19, 27). Because physiological parameters were not monitored by our protocol, this study provides no information regarding effects of obstruction of the rete mirabile on the animals' intracranial vascular physiology.

Angiographic Findings

The angiographic findings were consistent with progressive obliteration of the rete mira-

bile. The density of vessels outlined by the contrast material, as well as the size of the rete mirabile, decreased over the follow-up period. The time required for the angiographic findings to become apparent was clearly related to the radiosurgical dose. A high dose led to earlier obliteration than a low dose. Large variation among animals was observed. This is consistent with the findings in humans, in whom not all AVMs treated are obliterated in the same time frame (8) or respond in the same way to radiosurgery (3, 7, 9, 11). Variable responses to single-dose radiation in the same species has been well documented in vivo (28), and in vitro (29).

We found narrowing of the feeding and draining vessels of the rete mirabile. This finding was consistent with the fact that the vessel feeding the rete mirabile terminates in this structure. The narrowing of the draining vessel was analogous to AVM veins returning to normal size after treatment by radiosurgery. As drainage demand decreases, the draining vessel becomes atrophic. The animals were not allowed to survive long enough for us to observe total disappearance of both feeding and draining vessels. Because both retia were radiated, the neurologic findings were too severe to permit longer follow-up. A study in which only one rete is radiated and then followed up with long-term angiography may disclose the final fate of the feeding and draining vessels.

Histologic Findings

Progressive vessel wall thickening and thrombosis of the myriad vessels composing the AVM nidus are the hallmarks of the radiosurgical effect on these lesions (3). Intimal hyperplasia was observed in the rete mirabile radiated with doses larger than 20 Gy and followed up for more than 4 months. Intimal hyperplasia paralleled vascular thrombosis and was directly proportional to the radiosurgical dose. These histopathologic findings were corroborated by the longitudinal angiographic data demonstrating that the rete mirabile obliteration rate was proportional to the radiosurgical dose.

Microvascular response to radiosurgery observed in the rete mirabile represents a vascular repair reaction. This reaction, previously observed in experimental studies (28, 30–32), is common to microvessels in other sites of the body (29). Nilsson et al (32) studied the effect of gamma radiation to the basilar artery of the cat. They delivered doses higher than the doses applied in the present study and observed more necrosis of the basilar artery wall than thickening and vascular obliteration. Small vessels in the basilar adventitia and adjacent brain stem, most likely located in the "fall off" of the high doses applied, showed classical findings of hyalinization and obliteration. This repair reaction initiates with crumpling of endothelial cells, which partially or totally obliterate the lumen of small vessels. The endothelial cell crumpling is followed by intimal hyperplasia that evolves to atrophy of smooth muscle media cells. The media cells are finally replaced by hyaline and fibrinoid material (33–35). Structures surrounding the rete mirabile showed classical findings of radiation-induced edema and necrosis, as well as gliosis (36).

Structures surrounding the rete mirabile showed important histologic responses that were reflected in the animals' neurologic status. It was possible to define limiting doses where neurologic and histologic changes were not observed during the time frame of this study. This study defined the tolerance of these structures to radiosurgery, establishing important dose limits for further studies with this animal model.

Conclusion

This study delineates an important animal model with a natural structure that in many ways resembles an AVM response to radiosurgery. The histologic findings of hyperplasia, thrombosis, and inflammatory processes are similar to the response to radiosurgery described for AVMs. The time course of radiologic changes, as well as the neurologic deficits observed, also support this animal model as suitable for studies to elucidate effects of radiation to a conglomerate of microvasculature in the central nervous system. The size of the swine brain is ideal for imaging studies, such as magnetic resonance imaging, position emission tomography, and angiography. The effects of incremental doses of radiation alone or in association with embolization as shown on radiologic studies can be promptly related to histologic findings. The swine is a promising animal model for radiosurgical studies.

Acknowledgments

We are grateful to Lisa Shaker for her editorial assistance and to John Roberts for his technical support.

References

1. Drake CG. Cerebral arteriovenous malformations: considerations for and experience with surgical treatment of 166 cases. *Clin Neurosurg* 1979;26:145–208
2. Fults D, Kelly DL. Natural history of arteriovenous malformations of the brain: a clinical study. *Neurosurgery* 1984;15:658–662
3. Kjellberg RN, Hanamura T, Davis KR, et al. Bragg-peak proton-beam therapy for arteriovenous malformations of the brain. *N Engl J Med* 1983;309:269–274
4. Manchola IF, De Salles AAF, Foo TK, Ackerman RH, Candia GT, Kjellberg RN. Arteriovenous malformation hemodynamics: a transcranial Doppler study. *Neurosurgery* 1993;33:556–562
5. Ondra SL, Troupp H, George ED, et al. The natural history of symptomatic arteriovenous malformations of the brain: a 24-year follow-up assessment. *J Neurosurg* 1990;73:387–391
6. Betti OO, Munari C, Rosler R. Stereotactic radiosurgery with the linear accelerator: treatment of arteriovenous malformations. *Neurosurgery* 1989;24:311–321
7. Colombo F, Pozza F, Chiergo G, Casentini L, De Luca G, Francescon P. Linear accelerator radiosurgery of cerebral arteriovenous malformations: an update. *Neurosurgery* 1994;34:14–21
8. Friedman WA, Bova FJ, Mendenhall WM. Linear accelerator radiosurgery for arteriovenous malformations: the relationship of size and outcome. *J Neurosurg* 1995;82:180–189
9. Lunsford LD, Kondziolka D, Flickinger JC, et al. Stereotactic radiosurgery for arteriovenous malformation of the brain. *J Neurosurg* 1992;75:512–524
10. Steiner L, Leksell L, Greitz T, Forster DMC, Backlund EO. Stereotactic radiosurgery for cerebral arteriovenous malformations: report of a case. *Acta Chir Scand* 1972;138:459–462
11. Steiner L, Lindquist C, Cail W, Karlsson B, Steiner M. Microsurgery and radiosurgery in brain arteriovenous malformations. *J Neurosurg* 1993;79:647–652
12. Fabrikant JI, Lyman JT, Hosobuchi Y. Stereotactic heavy-ion Bragg peak radiosurgery for intra-cranial vascular disorders: method for treatment of deep arteriovenous malformations. *Br J Radiol* 1984;57:479–490
13. De Salles AAF. Complications after radiosurgery for brain AVM's. *J Neurosurg* 1990;76:559–560
14. Marks LB, Spencer DP. The influence of volume on tolerance of brain radiosurgery. *J Neurosurg* 1991;75:177–180
15. Solberg TD, De Salles AAF, Hovda D, Holly FE. A universal multimodality localization system for animal radiosurgery. *Acta Neurochir (Wein)* 1994;62:21–25
16. Lylyk P, Viñuela F, Vinters H, et al. Use of a new mixture for embolization of intracranial vascular malformations: preliminary experimental experience. *Neuroradiology* 1990;32:304–310
17. Winston KR, Lutz W. Linear accelerator as a neurosurgical tool for stereotactic radiosurgery. *Neurosurgery* 1988;22:454–464
18. Blat DR, Friedman WA, Bova FJ. Modification based on computed tomographic imaging in planning the radiosurgical treatment of arteriovenous malformations. *Neurosurgery* 1993;33:588–596
19. Daniel PM, Dawes JDK, Pichard MML. Studies of the carotid rete and its associated arteries. *Philos Trans R Soc Lond Biol* 1953;237:173–208
20. Spiegelmann R, Friedman WA, Bova FJ, Theele DP, Mickle JP. LINAC radiosurgery: an animal model. *J Neurosurg* 1993;78:638–644
21. Goetsch SJ, De Salles AAF, Solberg T, Holly FE, Selch MT, Bajada C. Treatment planning for stereotactic radiosurgery. In: De Salles AAF, Goetsch SH, eds. *Stereotactic Surgery and Radiosurgery*. Madison, Wis: Medical Physics; 1993:277–292
22. Lee DH, Wriedt CH, Kaufmann JCE. Evaluation of three embolic agents in the pig rete. *AJNR Am J Neuroradiol* 1989;10:773
23. Isoda K, Fukuda H, Takamura N, et al. Arteriovenous malformations of the brain: histological study and micrometric measurements of abnormal vessel. *Acta Pathol Jpn* 1981;31:883–893
24. De Salles AAF, Manchola I. CO_2 reactivity in arteriovenous malformations of the brain: a transcranial Doppler ultrasound study. *J Neurosurg* 1994;80:624–630
25. Spetzler RF, Hargraves RW, McCormick PW, Zabranski JM, Flom RA, Zimmerman RS. Relationship of perfusion pressure and size to risk of hemorrhage from arteriovenous malformations. *J Neurosurg* 1992;76:918–923
26. Massoud TF, Ji C, Viñuela F, et al. An experimental arteriovenous malformation model in swine, I: anatomic basis and construction technique. *AJNR Am J Neuroradiol* 1994;15:1537–1545
27. Dieguez G, Garcia AL, Conde MV, et al. In vitro studies of the carotid rete mirabile of artiodactyla. *Cardiovasc Res* 1987;33:143–154
28. Larsson B. Blood vessel changes following local irradiation of the brain with high-energy protons. *Acta Soc Upsaliensis* 1961;65:61–71
29. Marchese MJ, Hei TK, Zaider M, Bayne G, Kushner S. Radiation repair in human endothelial cells. *Int J Radiat Oncol Biol Phys* 1987;13:1857–1860
30. Lo EH, DeLaPaz RL, Frankel KA, et al. MRI and PET of delayed heavy-ion radiation injury in the rabbit brain. *Int J Radiat Oncol Biol Phys* 1991;20:689–696
31. Mori S, Tanaka R, Minakawa T. Effects of radiation on capillary endothelial cells derived from Mongolian gerbil brain. *Neurosurgery* 1991;29:658–662
32. Nilsson A, Wennerstrand J, Leksell D, Backlund EO. Stereotactic gamma irradiation of basilar artery in cat: preliminary experiences. *Acta Radiol Oncol* 1978;17:150–160
33. Dollinger MR, Lavine DM, Foye LV Jr. Myocardial infarction due to post-irradiation fibrosis of the coronary arteries: case of successfully treated Hodgkin's disease with lower esophageal involvement. *JAMA* 1966;195:316–319
34. Hopewell JW, Campling D, Calvo W, Reinhold HS, Wilkinson JH, Yeung TK. Vascular irradiation damage: its cellular basis and likely consequences. *Br J Cancer* 1986;53:181–191
35. Reinhold HS. The influence of radiation on blood vessels and circulation: structural changes in blood vessels. *Curr Top Radiat Res Q* 1974;10:59–74
36. Pearson HES. Incidental danger of x-ray therapy. *Lancet* 1958;1:222